OPAL Physics Note 291
May 12, 1997

Dijet Production in Photon-Photon Collisions at $\sqrt{s}_{\mathrm{ee}} = 161$ and 172 GeV

The OPAL Collaboration

Abstract

Dijet production is studied in collisions of quasi-real photons radiated by the LEP beams at e^+e^- centre-of-mass energies $\sqrt{s}_{\mathrm{ee}} = 161$ and 172 GeV. Jets are reconstructed using a cone jet finding algorithm. The inclusive two-jet cross-section and the angular distributions of direct and double-resolved processes are measured and compared to next-to-leading order perturbative QCD calculations and the prediction of the leading order Monte Carlo generators PYTHIA and PHOJET.

This note describes preliminary OPAL results to be submitted to the XVIII International Symposium on Lepton-Photon Interactions, Hamburg, 28 July - 1 August 1997, and to the International Europhysics Conference on High Energy Physics, Jerusalem, 19-26 August 1997

1 Introduction

We present a study of dijet production in two-photon collisions at $\sqrt{s}_{\mathrm{ee}} = 161$ and 172 GeV with an integrated luminosity of about 20 pb^{-1}. The cone jet finding algorithm was used to reconstruct jets. The production of dijet events in the collision of two quasi-real photons can be used to study the structure of the photon and different QCD predictions. At $\mathrm{e^+e^-}$ colliders the photons are emitted by the beam electrons[1]. Most of the photons carry only a small squared four-momenta Q^2 and can be considered to be quasi-real ($Q^2 \approx 0$). Accordingly the electrons are scattered with very small angles and are not detected. Events where one or both scattered electrons are detected are vetoed ("anti-tagged").

The interactions of the photons can be modelled by assuming that each photon can either interact directly or appear resolved through its fluctuations into hadronic states. The interactions of two photons are split into the direct process where two bare photons interact, a single-resolved process where a bare photon interacts with a parton (quark or gluon) of the other photon and a double-resolved process where partons of both photons interact. The possibility to distinguish between direct and resolved processes in dijet events has been demonstrated by OPAL [1].

In the centre-of-mass system of the interacting partons or bare photons the parton scattering angle θ^* is defined as the angle between the jet axis of the jets originating from the outgoing partons and the axis of the incoming partons or bare photons. Depending on the type of photon-photon interaction different matrix elements are involved. The matrix elements relevant to the different processes have been calculated in leading order (LO) [2,3]. The matrix element of the scattering between two bare photons is the one for process $\gamma\gamma \rightarrow q\bar{q}$. In double-resolved processes the matrix elements of quark-quark, gluon-quark and gluon-gluon scattering are involved [3]. These calculations predict different angular distributions of θ^*. In hadron-hadron and photon-hadron interactions the QCD predictions have been confirmed [4,5].

The measurement of inclusive jet cross-sections and the comparison with next to leading order (NLO) QCD calculations [6,7] and different photon structure functions can constrain the relatively unknown gluonic content of the photon [8]. In contrast to deep inelastic electron-photon scattering [9], which in leading order is only sensitive to the quark content of the photon, the gluon content of the photon can be tested, especially in the case of double-resolved processes, in the interaction of two almost real photons. Inclusive one-jet and two-jet cross-sections have been measured at an $\mathrm{e^+e^-}$ centre-of-mass energy of $\sqrt{s}_{\mathrm{ee}} = 58$ GeV at TRISTAN [8,10] and at an $\mathrm{e^+e^-}$ centre-of-mass energy of $\sqrt{s}_{\mathrm{ee}} = 130$ and 136 GeV at LEP [1].

This note extends a previous analysis [1] done at lower energies in which the same analysis strategy has been used and described in detail. In Section 2 the process kinematics and the Monte Carlo simulation are described. Section 3 contains a brief description of the OPAL detector and Section 4 the event selection and the jet finding. In Section 5 the inclusive two-jet cross-section is measured as a function of the parton scattering angle using two data samples of events with a large direct and double-resolved contribution. In Section 6 the inclusive two-jet cross-section is studied and compared to NLO calculations and different photon structure functions. Conclusions are given in Section 7.

[1] Positrons are also referred to as electrons.

2 Process kinematics and Monte Carlo simulation

The properties of the interacting photons are described by their negative squared four-momentum transfers Q_i^2 [2]. Each Q_i^2 is related to the electron scattering angle Θ_i' relative to the beam direction by

$$Q_i^2 = -(p_i - p_i')^2 \approx 2E_iE_i'(1 - \cos\Theta_i'), \tag{1}$$

where p_i and p_i' are the four-momenta of the beam electrons and the scattered electrons, respectively, and E_i and E_i' are their energies. Events with detected scattered electrons (single-tagged or double-tagged events) are excluded from the analysis. This anti-tagging condition defines an upper limit on Q_i^2 for both photons. This condition is met when the scattering angle Θ' of the electrons is less than $\Theta_{\max}$, where $\Theta_{\max}$ is the angle between the beam-axis and the inner edge of the detector. The hadronic final state is described by its invariant mass W. The spectrum of photons with an energy fraction y of the electron beams may be obtained by the Equivalent Photon Approximation (EPA) [11]:

$$f_{\gamma/e}(y) = \frac{\alpha}{2\pi}\left(\frac{1+(1-y)^2}{y}\log\frac{Q^2_{\max}}{Q^2_{\min}} - 2m_e^2 y\left(\frac{1}{Q^2_{\min}} - \frac{1}{Q^2_{\max}}\right)\right).$$

with α being the electromagnetic coupling constant. The minimum kinematically allowed squared four-momentum transfer $Q^2_{\min}$ is determined by the electron mass m_e:

$$Q^2_{\min} = \frac{m_e^2y^2}{1-y}.$$

The effective maximum four-momentum transfer $Q^2_{\max}$ is given by the anti-tagging condition, i. e. the case where both electrons remain undetected.

For the simulation of two-photon interactions the Monte Carlo generators PYTHIA [12] and PHOJET [13] have been used. More details can be found in Ref. [1]. All possible hard interactions relevant to two-photon interactions are included. The fragmentation is handled by JETSET 7.408. We separate photon-photon and electron-photon events in the Monte Carlo by requiring one photon with $Q^2 > 1$ GeV^2 for the electron-photon events. The electron-photon events with a scattered electron in the detector are single-tagged events. The rate of processes where both photons have $Q^2 > 1$ GeV^2 is negligibly small. All signal and background Monte Carlo samples were generated with full simulation of the OPAL detector [14]. They are analysed using the same reconstruction algorithms as are applied to the data.

3 The OPAL detector

A detailed description of the OPAL detector can be found in Ref. [15], and therefore only a brief account of the main features relevant to the present analysis will be given here.

The central tracking systems are located inside a solenoidal magnet which provides a uniform axial magnetic field of 0.435 T along the beam axis[2]. The magnet is surrounded by a lead glass

[2]In the OPAL coordinate system the x axis points towards the centre of the LEP ring, the y axis points upwards and the z axis points in the direction of the electron beam. The polar angle θ, the azimuthal angle ϕ and the radius r denote the usual spherical coordinates.

electromagnetic calorimeter (ECAL) and a hadronic calorimeter (HCAL) of the sampling type. Outside the HCAL, the detector is surrounded by a system of muon chambers. There are similar layers of detectors in the forward and backward endcaps. The region around the beam pipe on both sides of the detector is covered by the forward detectors and the silicon tungsten detectors.

The main tracking detector is the central jet chamber. It has 24 sectors with radial planes of 159 sense wires spaced by 1 cm. The transverse momenta p_T of tracks are measured with a precision parametrised by $\sigma_{p_T}/p_T = \sqrt{0.02^2 + (0.0015 \cdot p_T)^2}$ (p_T in GeV/c) in the central region $|\cos\theta| < 0.73$. For the most forward-going tracks used in this analysis, the transverse momentum resolution is approximately 10 %.

The ECAL has barrel and endcap sections, both constructed from lead glass blocks with a depth of 24.6 radiation lengths in the barrel and more than 22 radiation lengths in the endcaps. The endcaps cover the angular range from 200 to 630 mrad.

The forward calorimeters consist of cylindrical lead-scintillator calorimeters with a depth of 24 radiation lengths divided azimuthally into 16 segments. The electromagnetic energy resolution is about $18\%/\sqrt{E}$, where E is in GeV. The acceptance of the forward calorimeters covers the angular range from 47 to 140 mrad from the beam direction.

The silicon tungsten detectors [16] at each end of the OPAL apparatus cover an angular region between 33 and 59 mrad in front of the forward calorimeters. Each calorimeter consists of 19 layers of silicon detectors and 18 layers of tungsten, corresponding to a total of 22 radiation lengths. Each silicon layer consists of 16 wedge shaped silicon detectors. The electromagnetic energy resolution is about $24\%/\sqrt{E}$ (E in GeV).

4 Event selection and jet finding

The main background processes are e^+e^- annihilation events with hadronic final states. Electron-photon events and the process $e^+e^- \rightarrow e^+e^-\tau^+\tau^-$ are also considered to be background. Other background processes are found to be negligible. Two-photon events are selected with the following set of cuts:

- The sum of all energy deposits in the ECAL and the HCAL has to be less than 45 GeV. Calorimeter clusters have to pass an energy threshold of 100 or 250 MeV for different sections of the ECAL and 600 MeV or 2 GeV for the HCAL.
- The visible invariant hadronic mass, W_{ECAL}, measured in the ECAL has to be greater than 3 GeV.
- The missing transverse energy of the event measured in the ECAL and the forward calorimeters has to be less than 5 GeV. The energy of a cluster in the forward detector has to be larger than 1 GeV.
- At least 5 tracks must have been found in the tracking chambers. A track is required to have a minimum transverse momentum with respect to the z axis of 120 MeV/c, more

than 20 hits in the central jet chamber, and the innermost hit of the track must be inside a radius of 60 cm with respect to the z axis. The distance of closest approach to the beam spot must be less than 30 cm in the z direction and less than 2 cm in the $r\phi$ plane.

- No track in the event is allowed to have a momentum greater than 30 GeV/c.

- To remove events with scattered electrons in the forward calorimeters or in the silicon tungsten calorimeters, the total energy sum measured in the forward calorimeters has to be less than 50 GeV and the total energy sum measured in the silicon tungsten calorimeters less than 35 GeV. A cluster in the silicon tungsten detector is accepted if it has an energy of more than 1 GeV. This cut also reduces the contamination from multihadronic events with their thrust axis close to the beam direction.

- In order to estimate the z position of the vertex, we calculate the weighted average $\langle z_0 \rangle$ of the z coordinates of all tracks at the point of closest approach to the origin in the $r\phi$ plane using

$$\langle z_0 \rangle = \frac{\sum_i z_i \,/\, \sigma_{z\,i}^2}{\sum_i 1 \,/\, \sigma_{z\,i}^2},$$

where σ_{z_i} is the measurement error on z_i. The background due to beam-gas or beam-wall interactions is reduced by requiring $|\langle z_0 \rangle| < 10$ cm and $|Q| \leq 3$, where Q is the net charge of an event calculated from adding the charges of all tracks.

In the cone jet finding algorithm the total transverse energy $E_T^{\rm jet}$ of the jet inside the cone is the scalar sum of the transverse energies of its components [1,17]. In all parts of this analysis, a sum over the particles in the event or in a jet means a sum over charged tracks satisfying the quality cuts, and over all neutral clusters which are not associated with a charged track [1]. The transverse energy E_{T_i} of a particle is defined relative to the z axis of the detector with $E_{T_i} = E_i \sin\theta_i$. In the cone jet finding algorithm the information of the electromagnetic and hadronic calorimeters, the forward and silicon tungsten calorimeters, and all tracks is used. The value of $E_T^{\rm jet}$ must be greater than a certain minimum $E_T^{\rm min}$. The results of the cone jet finding algorithm depend on $E_T^{\rm min}$ and the cone size $R = \sqrt{(\Delta\eta)^2 + (\Delta\phi)^2}$ with the pseudorapidity $\eta = -\ln\tan(\theta/2)$ and the azimuthal angle ϕ. Here the values were chosen to be $R = 1$ and $E_T^{\rm min} = 2$ GeV. The jet pseudorapidity in the laboratory frame is required to be within $|\eta^{\rm jet}| < 2$. The reconstruction of jets with $|\eta^{\rm jet}|$-values in this range has been studied. It has been found that these jets are well reconstructed and are fully contained in the detector. This leads to a wider $\eta^{\rm jet}$-acceptance than in a previous analysis [1]. All results are given for jets with $E_T^{\rm jet} > 3$ GeV in order to be able to compare the results to perturbative QCD calculations.

We use data corresponding to an integrated luminosity of 20.0 pb^{-1}. After applying all cuts and requiring at least two jets 2681 events remain, 50 % of them at 161 GeV beam energy and 50 % at 172 GeV. The difference between the data taken at $\sqrt{s}_{\rm ee} = 161$ GeV and at 172 GeV is expected to be small. The mean Q^2 of the selected Monte Carlo events is 0.06 GeV^2. The visible hadronic invariant mass $W_{\rm vis}$ measured with all detector information is well described within the errors of the measurements by the Monte Carlo simulations. The average $W_{\rm vis}$ is about 28 GeV in data and about 27 GeV in the Monte Carlo, while in the Monte Carlo events the average generated invariant mass W for the same events is about 41 GeV.

About 83 % of all generated Monte Carlo events with at least two hadron jets in the range $E_T^{\rm jet} > 3$ GeV and $|\eta^{\rm jet}| < 2$ are selected after applying the detector simulation and the selection cuts to these events. The trigger efficiency for all selected Monte Carlo events with at least two reconstructed jets in the detector is close to 100 %. The number of background events is small, about 2 % in total. About 1.2 % of the events in the data sample are expected to be e^+e^- annihilation events with hadronic final states and 0.2 % electron-photon events.

5 Angular distributions in direct and resolved events

In leading order QCD, neglecting multiple parton interactions, two hard parton jets are produced in $\gamma\gamma$ interactions. In single- or double-resolved interactions, the two hard parton jets are expected to be accompanied by one or two remnant jets.

A pair of variables, x_γ^+ and x_γ^-, can be defined [18] which specify the fraction of the photon energy participating in the hard scattering:

$$x_\gamma^+ = \frac{\sum\limits_{\rm jets=1,2} (E+p_z)}{\sum\limits_{\rm hadrons} (E+p_z)} \quad \text{and} \quad x_\gamma^- = \frac{\sum\limits_{\rm jets=1,2} (E-p_z)}{\sum\limits_{\rm hadrons} (E-p_z)}, \tag{2}$$

where p_z is the momentum component along the z axis of the detector and E is the energy of the jets or hadrons. These variables give some separation between the direct and the resolved events [1]. We use events with at least two jets to calculate x_γ^+ and x_γ^-. If an event contains more than two jets, the two jets with the highest $E_T^{\rm jet}$ values are taken. The variables x_γ^+ and x_γ^- are measured using all tracks and calorimeter clusters that were used in the jet finding algorithm.

Ideally, for direct events without remnant jets, the total energy of the event is contained in the two jets, i. e. $x_\gamma^+ = 1$ and $x_\gamma^- = 1$, whereas for single-resolved events either x_γ^+ or x_γ^- and for double-resolved events both values x_γ^+ and x_γ^- are expected to be much smaller than 1. Samples with large direct and double-resolved contributions can be separated by requiring both x_γ^+ and x_γ^- to be larger than 0.8 (denoted as $x_\gamma^\pm > 0.8$) or both values to be smaller than 0.8 (denoted as $x_\gamma^\pm < 0.8$), respectively. Details about the separation between different event classes can be found in Ref. [1]. In the PYTHIA Monte Carlo 87 % of all events in the region $x_\gamma^\pm > 0.8$ originate from direct interactions and 81 % of all events in the region $x_\gamma^\pm < 0.8$ originate from double-resolved interactions.

The transverse energy flow around the jet axis for double-resolved events is expected to show additional activity outside the jet due to the photon remnant compared to the direct events. Figure 1 therefore shows the transverse energy flow

$$\frac{1}{N_{\rm jet}} \frac{{\rm d}E_T}{{\rm d}(\Delta\eta')} \tag{3}$$

around the jets with respect to the jet direction for data samples with different $x_\gamma^\pm$ cuts. The pseudorapidity difference is defined by:

$$\Delta\eta' = k(\eta - \eta^{\rm jet}).$$

The factor k is chosen event-by-event to be $k = +1$ for events with $x_\gamma^+ > x_\gamma^-$ and $k = -1$ for events with $x_\gamma^+ < x_\gamma^-$. As a consequence, there is always more of the remnant found at $\Delta\eta' < 0$ and the enhancement due to the additional transverse energy flow observed at negative and positive $\Delta\eta'$ is asymmetric. No correction for acceptance or resolution effects has been applied. The energy flow is integrated over $|\Delta\phi| < \pi/2$. The jets in the data sample with $x_\gamma^\pm > 0.8$ are more collimated and there is almost no activity outside the jet whereas the transverse energy flow of two-jet events with $x_\gamma^\pm < 0.8$ shows activity outside the jets around $|\Delta\eta'| > 1$. The energy flow outside the jet is well modelled by PYTHIA whereas PHOJET overestimates the energy flow in this region.

The measurement of x_γ^+ and x_γ^- and the transverse energy flows depend on the same detector information. The angular distribution of the jets can be used to check the separation between the different event classes using a variable which is not directly correlated to the definition of x_γ^+ and x_γ^-. In the dijet centre-of-mass frame one expects different angular distributions for direct and double-resolved events. An estimator of the angle between the jets and the parton-parton axis in the dijet centre-of-mass frame can be formed from their pseudorapidities. The variable $\cos\theta^*$ is calculated as

$$\cos\theta^* = \tanh\left(\frac{\eta^{\mathrm{jet1}} - \eta^{\mathrm{jet2}}}{2}\right).$$

The two jets are assumed to be back to back in ϕ and have equal values of E_T^{jet}. Since the ordering of the jets is arbitrary, only $|\cos\theta^*|$ can be measured. The matrix elements of elastic parton-parton scattering processes have been calculated in LO [2,3]. For a given parton centre-of-mass energy the cross-sections vary only with the parton scattering angle θ^*. The dominating process in direct interactions $\gamma\gamma \to q\overline{q}$ has an angular dependence of approximately $\propto (1 - |\cos\theta^*|)^{-1}$. In double-resolved processes the contributing matrix elements predict an angular dependence of approximately $\propto (1 - |\cos\theta^*|)^{-2}$ [2,3].

The invariant mass of the two-jet system is calculated as

$$M_{jj} = \frac{2E_T^{\mathrm{jet}}}{\sqrt{1 - |\cos\theta^*|^2}}.$$

The cut on E_T^{jet} restricts the accessible range of values of $|\cos\theta^*|$. The M_{jj}-distribution of the data compared to the Monte Carlo expectations is shown in Fig. 2a. The drop of M_{jj} below 10 GeV is caused by the E_T^{jet} cut. Requiring that M_{jj} is larger than 12 GeV ensures that values of $|\cos\theta^*| < 0.85$ are not biased by the E_T^{jet} cut.

The boost of the two-jet system in the z direction is defined by

$$\bar{\eta} = \frac{\eta^{\mathrm{jet1}} + \eta^{\mathrm{jet2}}}{2}.$$

The $\bar{\eta}$-distribution is shown in Fig. 2b without applying a cut on M_{jj}. The detector resolution on $|\cos\theta^*|$ deteriorates significantly for events with $|\bar{\eta}|$ larger than 1. These events were therefore rejected by requiring $|\bar{\eta}| < 1$. The number of dijet events predicted by PYTHIA is about 30 % too low, whereas the PHOJET prediction agrees well with the data. After additionally requiring $M_{jj} > 12$ GeV and $|\bar{\eta}| < 1$ in the data 159 events remain with $x_\gamma^\pm > 0.8$ and 320 events with $x_\gamma^\pm < 0.8$.

Table 1 shows the measured cross-sections for data samples with large direct and large double-resolved contributions according to the separation with x_γ^+ and x_γ^-. To measure the cross-section a bin-by-bin correction was applied. The systematic uncertainty on the jet cross-sections given in this section is determined by varying the energy scale of the ECAL in the Monte Carlo simulation by ± 5 %. The dependence on the Monte Carlo models used is taken into account by adding the difference between the results obtained with PYTHIA, which are taken to be the central values, and PHOJET to the systematic error. The contributions of these two errors to the total systematic error are of similar size.

Figure 3 shows the $|\cos\theta^*|$-distribution of events with $x_\gamma^\pm > 0.8$ and of events with $x_\gamma^\pm < 0.8$. The data points are normalised to have an average value of 1 in the first three bins and are plotted at the centre of the bins. The error bars show the statistical and the systematic errors added in quadrature. In the Monte Carlo events about 10 % of the processes with $x_\gamma^\pm > 0.8$ are resolved and about 15 % of the processes with $x_\gamma^\pm < 0.8$ are direct nearly independent of $|\cos\theta^*|$. The $|\cos\theta^*|$ distribution is not corrected for these impurities. The events with $x_\gamma^\pm > 0.8$ show a small rise with $|\cos\theta^*|$, whereas the events with $x_\gamma^\pm < 0.8$ show a much stronger rise in $|\cos\theta^*|$, as expected from the QCD calculations. The data points of the events with $x_\gamma^\pm < 0.8$ are compared with the prediction of a QCD matrix element calculation of the interaction of quarks or gluons in the photon. The curves are normalised to have a value of 1 at $|\cos(0)|$. The process $gg \rightarrow gg$ is expected to provide the largest contribution [19]. The matrix elements with a relevant contribution to the cross-section where antiquarks are involved instead of quarks show a similar behaviour as the examples shown. The contribution of the different processes to all double-resolved events depends on the parametrisation of the photon structure function. The events with $x_\gamma^\pm > 0.8$ are compared with the calculation of the process $\gamma\gamma \rightarrow q\overline{q}$. The QCD matrix element calculations agree well with the data points of the data samples with large direct and large double-resolved contribution.

6 Inclusive two-jet cross-sections

The inclusive two-jet cross-section in the range $|\eta^{\mathrm{jet}}| < 2$ and $E_T^{\mathrm{jet}} > 3$ GeV is measured using the cone jet finding algorithm with a cone size $R = 1$. In order to obtain jet cross-sections which can be compared to theoretical calculations, we use the unfolding program RUN [20] to correct for the selection cuts, the resolution effects of the detector and the background from non-signal processes. The same technique was used as described in [1]. To improve the results of the unfolding program in the region $E_T^{\mathrm{jet}} > 3$ GeV, migration effects from jets at low E_T^{jet} must be taken into account. Therefore the jets are actually found with $E_T^{\mathrm{min}} = 2$ GeV and the unfolding is performed in the full $E_T^{\mathrm{jet}} > 2$ GeV range. The reduction in the measured cross-section resulting from the use of $E_T^{\mathrm{min}} = 3$ GeV contributes especially at low E_T values.

In Fig. 4, the inclusive two-jet cross-section is shown as a function of E_T^{jet}. The determination of the average transverse energy $\langle E_T^{\mathrm{jet}} \rangle$ plotted on the abscissa is based on the method proposed in Ref. [21]. As in the calculation of x_γ^+ and x_γ^- in events with more than two jets, only the two jets with the highest E_T^{jet} values are taken. The error bars show the statistical and the systematic errors added in quadrature. The bin sizes, which are indicated by the vertical lines at the top of the figures, approximately reflect the experimental resolution. The results are summarised in Table 2. The systematic errors are calculated in the same way as in Section 5. An additional error from the unfolding procedure is taken into account.

The $E_T^{\rm jet}$ distribution is compared to an NLO perturbative QCD calculation of the inclusive two-jet cross-section by Kleinwort and Kramer [6] who use the NLO GRV parametrisation of the photon structure function [23]. Their calculation was repeated for the kinematic conditions of this analysis. All scales are chosen to be equal to $E_T^{\rm jet}$. The strong coupling constant $\alpha_{\rm s}$ is calculated from the two-loop formula with $\Lambda^{(5)}_{\overline{\rm MS}} = 130$ MeV. This value is also used in the GRV parametrisation. The direct, single- and double-resolved parts and their sum are shown separately. The data points are in good agreement with the calculation except in the first bin where the calculation predicts a much higher cross-section. The resolved cross-sections dominate in the region $E_T^{\rm jet} \lesssim 8$ GeV, whereas, at high $E_T^{\rm jet}$ the direct cross-section is largest.

The NLO QCD calculation gives the jet cross-section for massless partons, whereas the experimental jet cross-sections are measured for hadrons. The uncertainties due to the modelling of the hadronisation process have not been taken into account. Figure 5 shows the LO and NLO calculations with massless partons and the prediction of PYTHIA using GRV on parton and hadron level. For this comparison the PYTHIA events were generated turning off initial and final state QCD and QED radiation and multiple interactions. The jets found on the parton and on the hadron level were then compared in order to estimate the effect of the correction. The difference due to fragmentation mainly contributes at low $E_T^{\rm jet}$ values. This correction would increase the cross-section by about a factor of 1.2 to 1.3 in agreement with recent results [1,22].

The inclusive two-jet cross-section, which is dominated by the low $E_T^{\rm jet}$ events, depend on the parton density function of the photon which mainly differ in the assumptions on the gluon part of the photon. This leads to different predictions of the inclusive two-jet cross-section especially for double-resolved events. The inclusive two-jet cross-section as a function of $|\eta^{\rm jet}|$ is shown in Fig. 6a for the whole data sample and in Fig. 6b for events with a large double-resolved contribution after requiring $x_\gamma^\pm < 0.8$. The results are summarised in Table 3. The average $\langle\eta^{\rm jet}\rangle$ values are consistent with being at the centre of the bins. Within the statistical and systematic uncertainties of the measurement, the distributions are nearly independent of $|\eta^{\rm jet}|$ with a small drop towards $|\eta^{\rm jet}| = 2$ in the kinematic range shown, in agreement with the expectations of the Monte Carlo models. The inclusive two-jet cross-section predicted by the two Monte Carlo models differ significantly even if the same photon structure function (here GRV LO) is used. This model dependence reduces the sensitivity to the parametrisation of the photon structure function. Different parametrisations were used as input to the PYTHIA simulation. The GRV-LO and SaS-1D parametrisations [23,24] describe the data equally well, but the LAC1 parametrisation [25] overestimates the inclusive two-jet cross-section significantly with PYTHIA and PHOJET as observed at lower energies [1]. The inclusive two-jet cross-section of events with a large contribution of direct events with $x_\gamma^\pm > 0.8$ is well described by all photon structure functions SaS-1D, GRV and LAC1.

7 Conclusions

We have measured dijet production in photon-photon interactions with the OPAL detector at e^+e^- centre-of-mass energies $\sqrt{s}_{ee}$ of 161 and 172 GeV. Jets were identified using a cone jet finding algorithm with $R = 1$ in the kinematic range $E_T^{jet} > 3$ GeV and $|\eta^{jet}| < 2$. Two-jet events originating mainly from direct and double-resolved photon interactions were separated experimentally using the variables x_γ^+ and x_γ^-. The Monte Carlo models PYTHIA and PHOJET describe the shape of the transverse energy flow around the jets reasonably well.

The distribution of the parton scattering angle θ^* using the variable $|\cos\theta^*|$ has been measured. Data samples with large direct and double-resolved contributions have been compared to the relevant QCD matrix element calculations. The strong rise in the $|\cos\theta^*|$ distribution of the data sample with a large double-resolved contribution at high $|\cos\theta^*|$ as expected from QCD has been observed. The less steep $|\cos\theta^*|$ distribution of the data sample with a large contribution of direct events is also in good agreement with the QCD calculation.

The inclusive two-jet cross-sections were measured as a function of E_T^{jet} and $|\eta^{jet}|$. The E_T^{jet} dependent two-jet cross-section is in good agreement with next-to-leading order QCD calculations by Kleinwort and Kramer [6] above $E_T^{jet} = 4$ GeV. In the first bin between 3 and 4 GeV, where experimental errors and hadronisation effects are expected to be largest the calculation predicts a much larger cross-section as maeasured.

The inclusive two-jet cross-section is dominated by the resolved processes in the low E_T^{jet} region. Large differences between the calculated jet cross-sections in PYTHIA and PHOJET reduce the sensitivity to the parametrisation of the photon structure function. Given this model dependence, the GRV-LO and SaS-1D parametrisations describe the cross-section of all two-jet events and of a data sample with a large contribution from double-resolved events equally well. The LAC1 parametrisation overestimates the inclusive two-jet cross-section significantly.

Acknowledgements

We thank R. Engel and T. Sjöstrand for providing the Monte Carlo code and for many useful discussions and G. Kramer and T. Kleinwort for providing the NLO calculations.

References

[1] OPAL Collaboration, K. Ackerstaff et al., Z. Phys. C73 (1997) 433.

[2] H. Kolanoski, *Two-Photon Physics at e^+e^- Storage Rings*, Springer-Verlag (1984).

[3] B. L. Combridge et al., Phys. Lett. B70 (1977) 234;
D. W. Duke and J. F. Owens, Phys. Rev. D26 (1982) 1600.

[4] CDF Collaboration, F. Abe et al., Phys. Rev. Lett. 77 (1996) 5336.

[5] ZEUS Collaboration, M. Derrick et al., DESY 96-094 (1996);
ZEUS Collaboration, M. Derrick et al., Phys. Lett. B348 (1995) 665;
ZEUS Collaboration, M. Derrick et al., Phys. Lett. B342 (1995) 417.

[6] T. Kleinwort, G. Kramer, DESY-96-035 (1996);
T. Kleinwort, G. Kramer, Phys. Lett. B370 (1996) 141;
T. Kleinwort, G. Kramer, private communication.

[7] P. Aurenche, J. Ph. Guillet, M. Fontannaz, Y. Shimizu, J. Fujimoto and K. Kato, Progr. Theor. Phys. 92 (1994) 175;
P. Aurenche, J. Ph. Guillet, M. Fontannaz, Y. Shimizu, J. Fujimoto and K. Kato, Proc. Workshop on Two-Photon Physics at LEP and HERA, Lund, Sweden (May 1994) 269.

[8] AMY Collaboration, B. J. Kim et al., Phys. Lett. B325 (1994) 248.

[9] OPAL Collaboration, R. Akers et al., Z. Phys. C61 (1994) 199;
OPAL Collaboration, K. Ackerstaff et al., CERN-PPE 96/155;
DELPHI Collaboration, P. Abreu et al., Z. Phys. C69 (1996) 223.

[10] TOPAZ Collaboration, H. Hayashii et al., Proc. 10th Workshop on Gamma-Gamma Collisions and Related Processes, Sheffield, UK (April 1995) 133;
TOPAZ Collaboration, H. Hayashii et al., Phys. Lett. B314 (1993) 149.

[11] For a recent discussion see: G. A. Schuler, CERN-TH/96-297.

[12] T. Sjöstrand, Comp. Phys. Commun. 82 (1994) 74;
T. Sjöstrand, LUND University Report, LU-TP-95-20 (1995).

[13] R. Engel and J. Ranft, Phys. Rev. D54 (1996) 4244;
R. Engel, Z. Phys. C66 (1995) 203.

[14] J. Allison et al., Nucl. Instrum. Methods A317 (1992) 47.

[15] OPAL Collaboration, K. Ahmet et al., Nucl. Instrum. Methods A305 (1991) 275;
P. P. Allport et al., Nucl. Instrum. Methods A346 (1994) 476;
P. P. Allport et al., Nucl. Instrum. Methods A324 (1993) 34.

[16] B. E. Anderson et al., IEEE Transactions on Nuclear Science 41 (1994) 845.

[17] OPAL Collaboration, R. Akers et al., Z. Phys. C63 (1994) 197.

[18] L. Lönnblad and M. Seymour (convenors), $\gamma\gamma$ *Event Generators*, in "Physics at LEP2", CERN 96-01, eds. G. Altarelli, T. Sjöstrand and F. Zwirner, Vol. 2 (1996) 187.

[19] M. Erdmann, DESY-96-090 (1996).

[20] V. Blobel, DESY-84-118 (1984);
V. Blobel, Proc. 1984 CERN School of Computing, Aiguablava, Spain, CERN 85-09 (September 1984);
V. Blobel, *The RUN manual, Regularized Unfolding for High-Energy Physics Experiments*, program manual, unpublished.

[21] G. D. Lafferty and T. R. Wyatt, Nucl. Instrum. Methods A355 (1995) 541.

[22] M. Klasen, G. Kramer and S. G. Salesch, Z. Phys. C68 (1995) 113.

[23] M. Glück, E. Reya and A. Vogt, Phys. Rev. D46 (1992) 1973;
M. Glück, E. Reya and A. Vogt, Phys. Rev. D45 (1992) 3986.

[24] G. A. Schuler and T. Sjöstrand, Z. Phys. C68 (1995) 607.

[25] H. Abramowicz, K. Charchula and A. Levy, Phys. Lett. B269 (1991) 458.

$\lvert\cos\theta^*\rvert$	$d\sigma/d\lvert\cos\theta^*\rvert$ (pb)	
	resolved($x_\gamma^\pm < 0.8$)	direct($x_\gamma^\pm > 0.8$)
0.000 - 0.106	$5.1 \pm 1.6 \pm 0.3$	$9.5 \pm 2.1 \pm 2.4$
0.106 - 0.213	$5.1 \pm 1.6 \pm 0.8$	$4.2 \pm 1.4 \pm 1.3$
0.213 - 0.319	$7.3 \pm 1.9 \pm 0.6$	$3.0 \pm 1.2 \pm 0.4$
0.319 - 0.425	$6.3 \pm 1.7 \pm 0.3$	$9.8 \pm 2.2 \pm 1.3$
0.425 - 0.531	$6.8 \pm 1.8 \pm 0.2$	$11.9 \pm 2.4 \pm 1.6$
0.531 - 0.638	$7.0 \pm 1.8 \pm 0.5$	$17.2 \pm 2.9 \pm 1.5$
0.638 - 0.744	$8.1 \pm 2.0 \pm 0.6$	$29.6 \pm 3.7 \pm 2.9$
0.744 - 0.850	$15.6 \pm 2.7 \pm 1.3$	$57.8 \pm 5.2 \pm 5.4$

Table 1: Differential two-jet cross-section as a function of $\lvert\cos\theta^*\rvert$. The cross section is shown for events with $x_\gamma^\pm < 0.8$ and for events with $x_\gamma^\pm > 0.8$. The first error is statistical and the second error is systematic.

$E_T^{\rm jet}$ (GeV)	$\langle E_T^{\rm jet}\rangle$ (GeV)	$d\sigma/dE_T^{\rm jet}$ (pb/GeV)
3.0– 4.0	3.47 ± 0.01	$133 \pm 3 \pm 14$
4.0– 5.0	4.47 ± 0.01	$77.5 \pm 2.2 \pm 7.5$
5.0– 6.5	5.69 ± 0.01	$27.3 \pm 0.9 \pm 3.9$
6.5– 8.5	7.42 ± 0.01	$12.4 \pm 0.5 \pm 1.4$
8.5–11.0	9.64 ± 0.01	$4.4 \pm 0.28 \pm 0.72$
11.0–15.0	12.78 ± 0.02	$1.28 \pm 0.13 \pm 0.32$
15.0–20.0	17.22 ± 0.02	$0.16 \pm 0.04 \pm 0.15$

Table 2: The inclusive two-jet cross-section as a function of $E_T^{\rm jet}$. The first error is statistical and the second error is systematic.

$\lvert\eta^{\rm jet}\rvert$	$\mathrm{d}\sigma/\mathrm{d}\lvert\eta^{\rm jet}\rvert$ (pb)	
	no $x_\gamma^\pm$ cut	resolved($x_\gamma^\pm < 0.8$)
0.0 - 0.4	$184.7 \pm 5.5 \pm 21.4$	$132.5 \pm 5.1 \pm 19.3$
0.4 - 0.8	$183.5 \pm 5.0 \pm 18.0$	$120.6 \pm 4.3 \pm 15.6$
0.8 - 1.2	$143.4 \pm 4.3 \pm 16.8$	$88.4 \pm 3.6 \pm 15.5$
1.2 - 1.6	$135.6 \pm 4.7 \pm 15.0$	$89.3 \pm 4.2 \pm 14.0$
1.6 - 2.0	$143.5 \pm 5.6 \pm 15.4$	$108.1 \pm 5.4 \pm 14.8$

Table 3: The inclusive two-jet cross-section as a function of $\eta^{\rm jet}$. The inclusive two-jet cross-section is shown for all two-jet events and for a data sample with a large contribution from double-resolved events after requiring $x_\gamma^\pm < 0.8$. The first error is statistical and the second error is systematic.

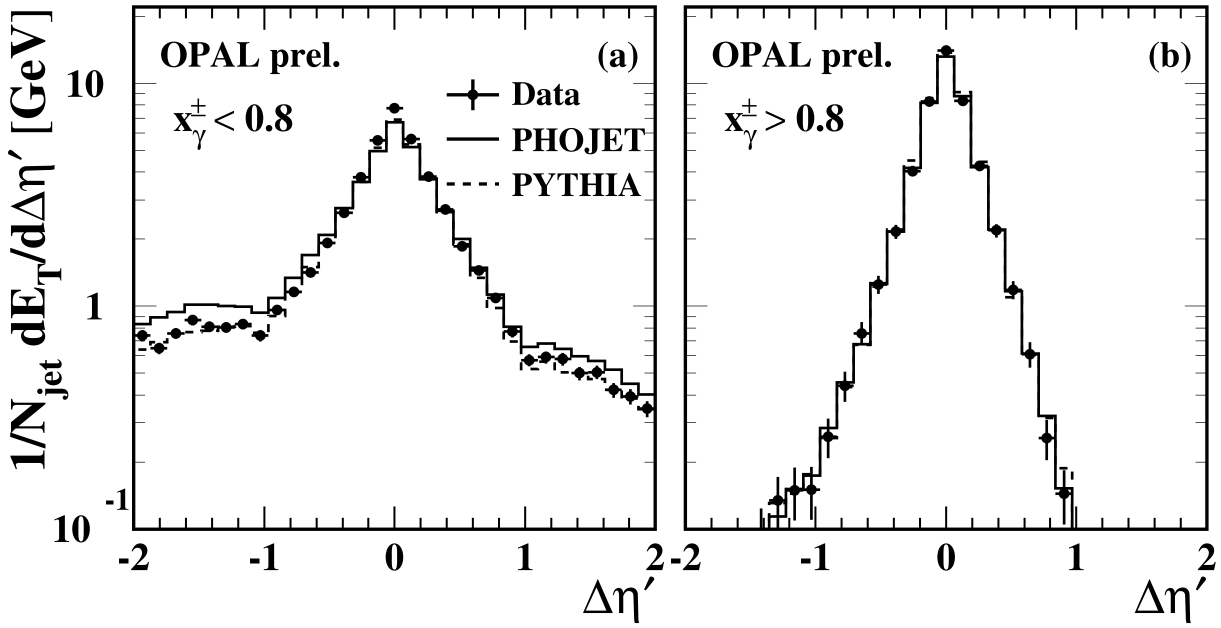

Figure 1: Uncorrected energy flow transverse to the beam direction measured relative to the direction of each jet in two-jet events. Jets from data samples with a large contribution of (a) double-resolved and (b) direct events according to their x_γ^+ and x_γ^- values are shown. The energy flow is integrated over $|\Delta\phi| < \pi/2$. Statistical errors only are shown. The data (dots) are compared to the PHOJET (continuous line) and PYTHIA (dashed line) simulations.

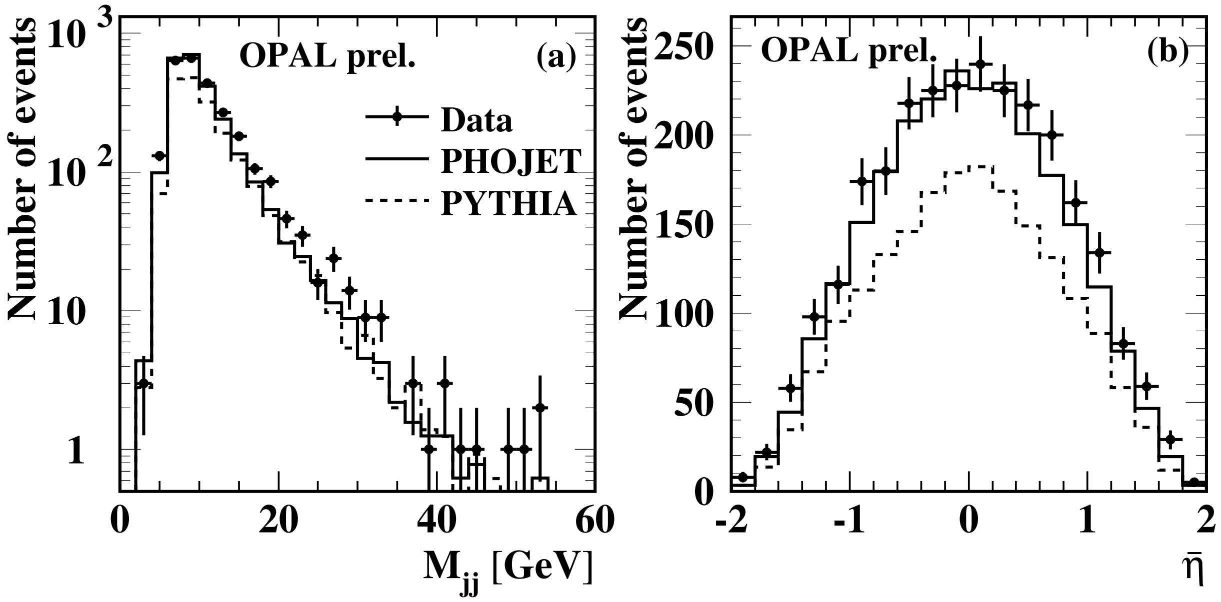

Figure 2: (a) Uncorrected invariant mass of the two-jet system. (b) Distribution of $\bar{\eta}$. The data (dots) are compared to the PHOJET (continuous line) and PYTHIA (dashed line) simulations.

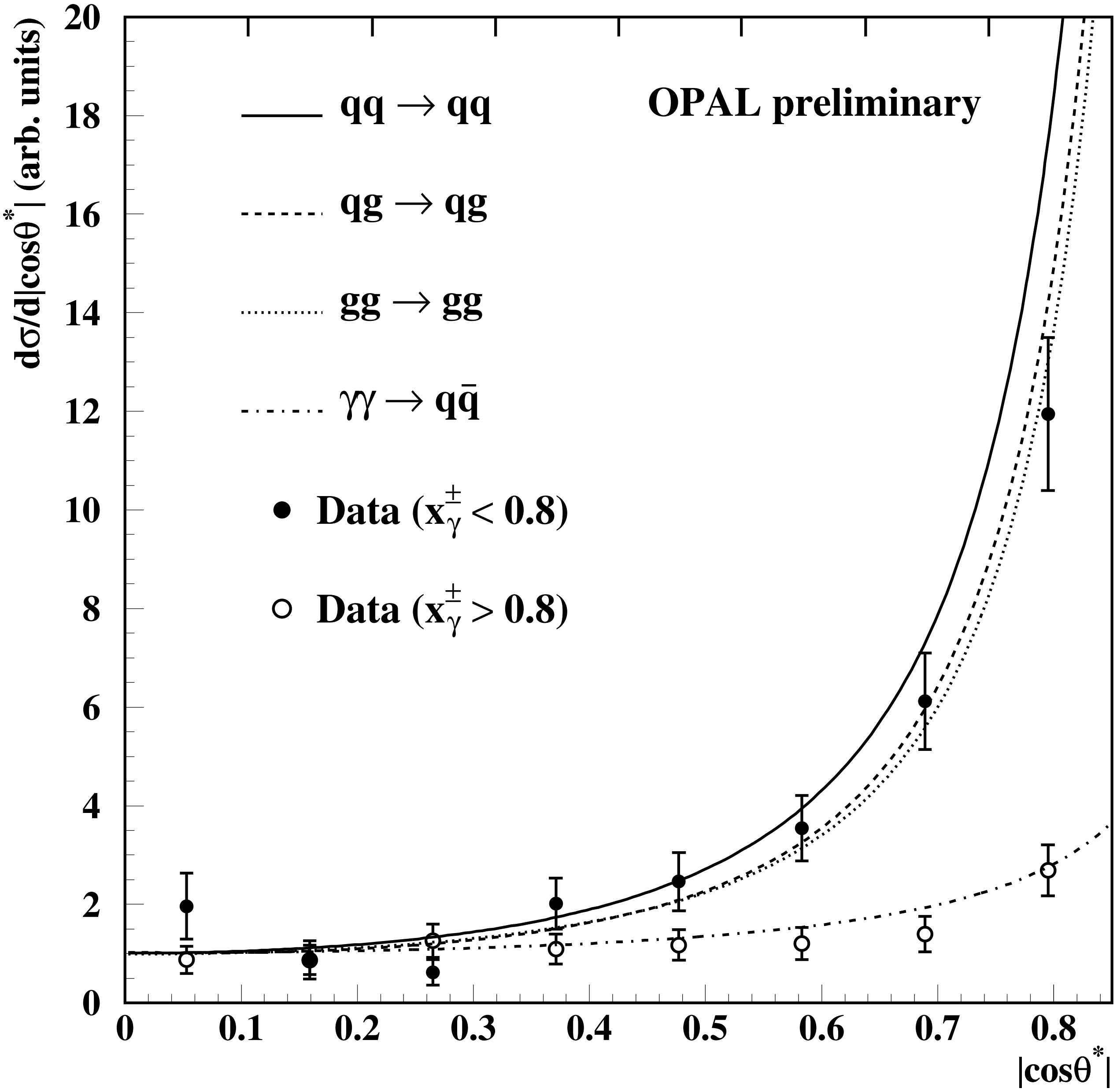

Figure 3: Angular distribution of events with large direct and large double-resolved contributions according to the separation with x_γ^+ and x_γ^-. The data are compared to QCD matrix element calculations [2, 3]. The data are normalised to have an average value of 1 in the first three bins and the curves are normalised to be 1 at $\cos(0)$. *The open circles show the distribution of events with $x_\gamma^\pm > 0.8$, the full circles show the distribution of events with $x_\gamma^\pm < 0.8$.*

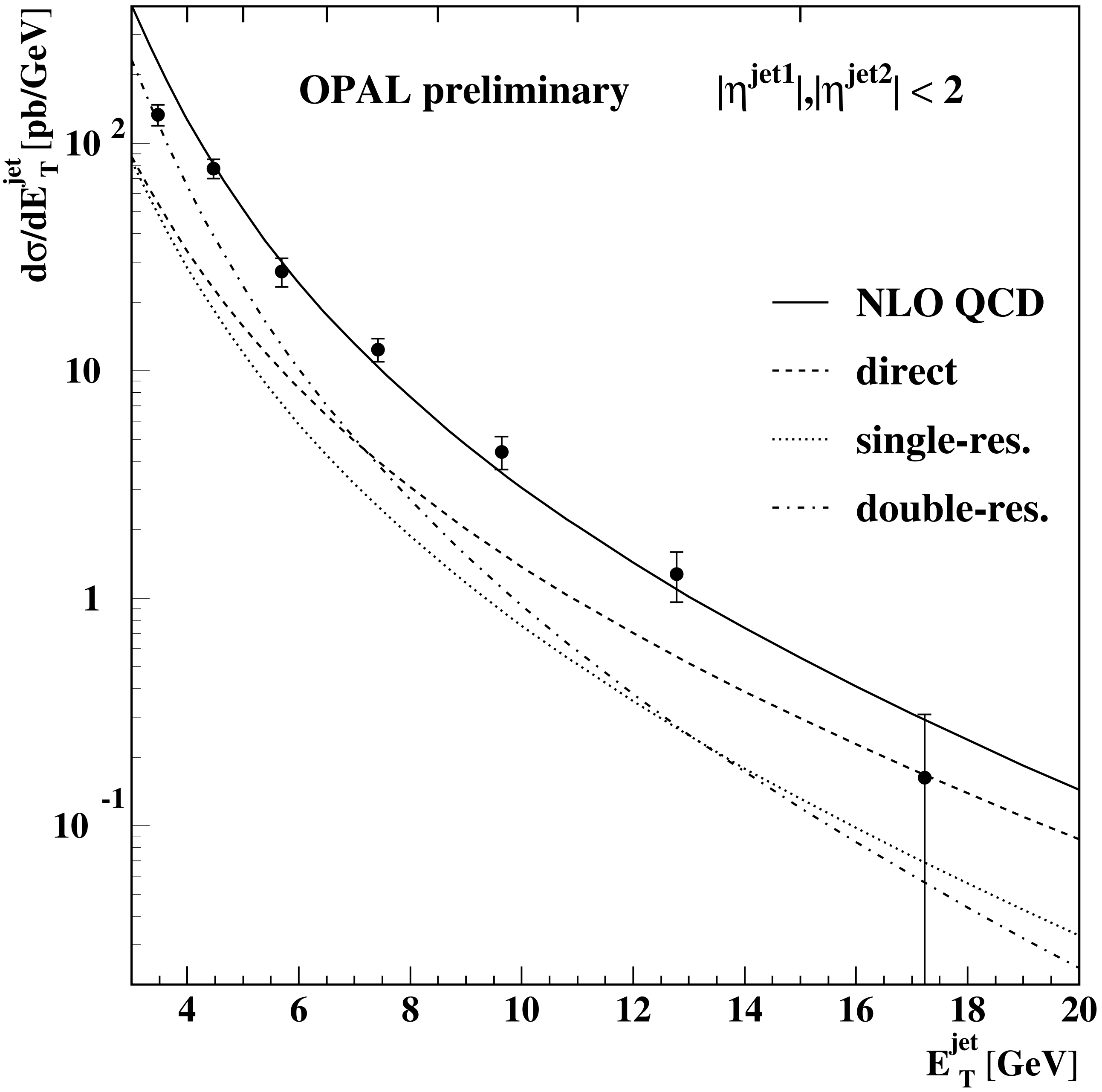

Figure 4: The inclusive two-jet cross-section as a function of $E_T^{\rm jet}$ for jets with $|\eta^{\rm jet}| < 2$ compared to the NLO calculation by Kleinwort and Kramer [6]. The direct, single-resolved and double-resolved cross-sections and the sum (continuous line) are shown separately.

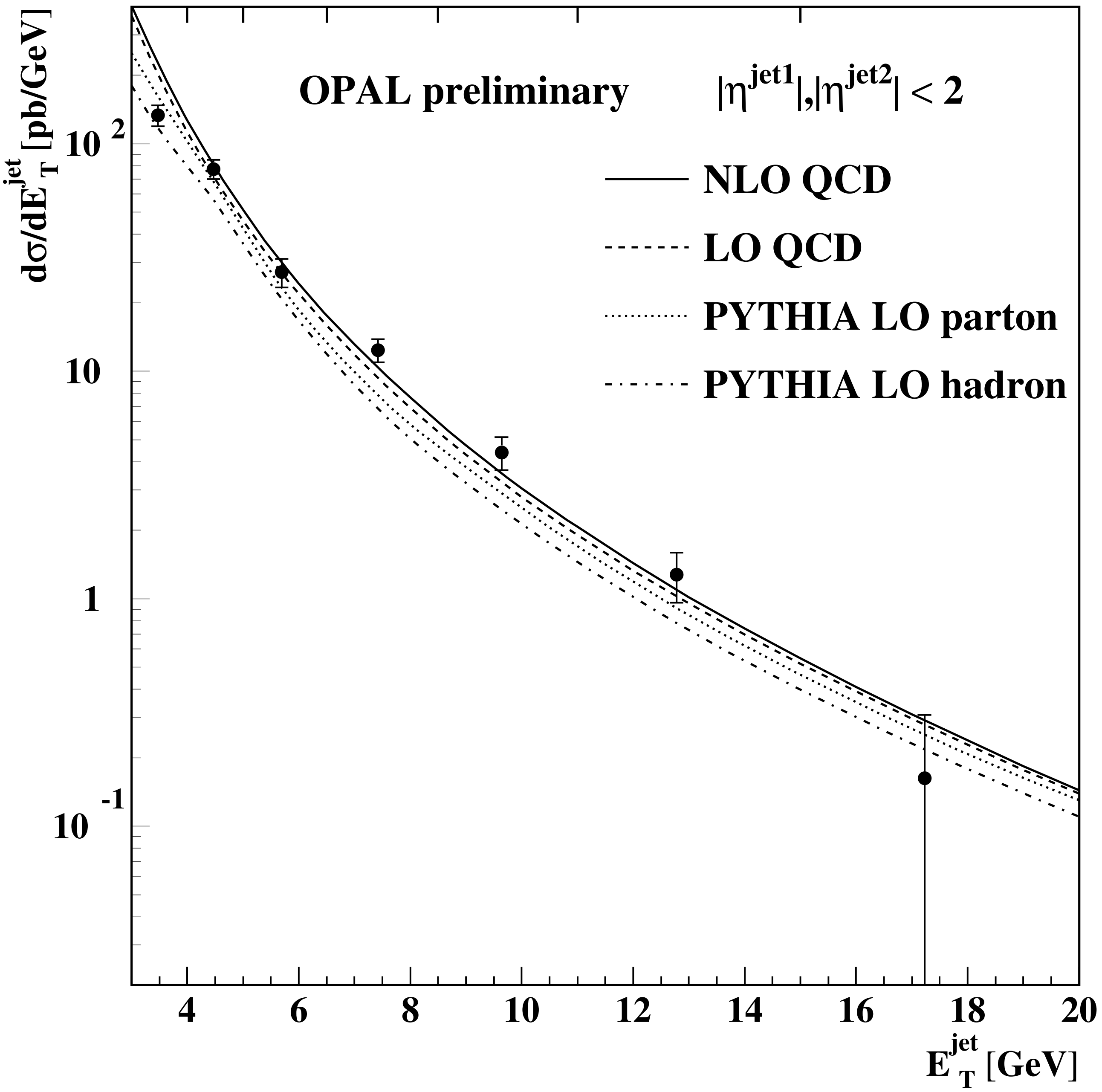

Figure 5: The inclusive two-jet cross-section as a function of $E_T^{\rm jet}$ for jets with $|\eta^{\rm jet}| < 2$ compared to the NLO calculation and the LO calculation by Kleinwort and Kramer [6]. The PYTHIA prediction in LO at parton and hadron level are also shown.

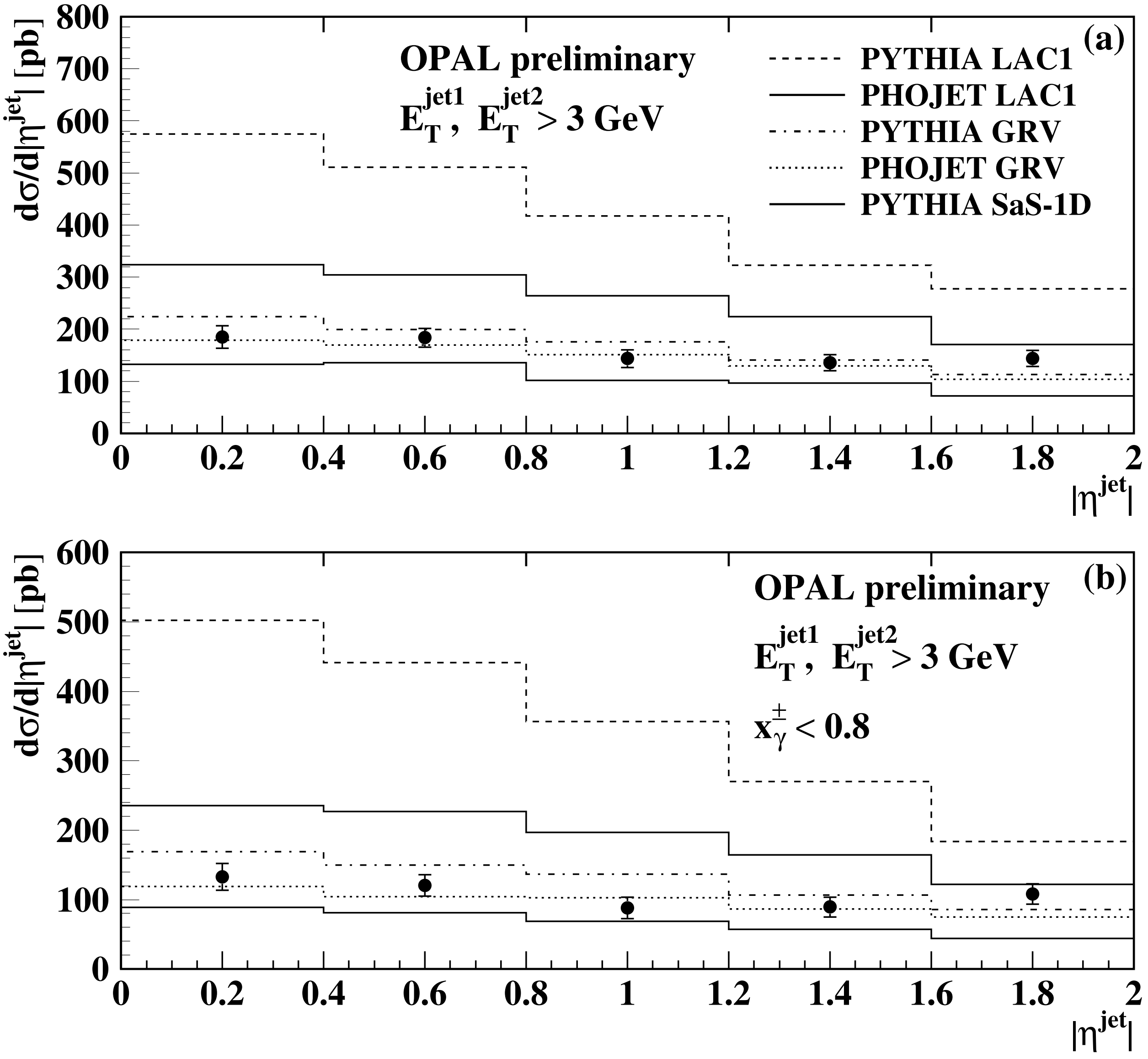

Figure 6: The inclusive two-jet cross-section as a function of $|\eta^{\rm jet}|$ for jets with $E_T^{\rm jet} > 3$ GeV (a) for all events and (b) for events with a large contribution of double-resolved events after requiring $x_\gamma^\pm < 0.8$.